Nov 9th, 12:00 AM - 12:00 AM

Identifying Shear Buckling Coefficients for Channels with Rectangular Web Stiffeners using the Generalised cFSM

Morgan A. Rendall

Gregory J. Hancock

Kim J. R. Rasmussen

Wei-Wen Yu International Specialty Conference on Cold-Formed Steel Structures
Baltimore, Maryland, U.S.A, November 9 & 10, 2016

Identifying shear buckling coefficients for channels with rectangular web stiffeners using the generalised *c*FSM

Morgan A. Rendall[1], Gregory J. Hancock[2] and Kim J.R. Rasmussen[3]

Abstract

The Direct Strength Method (DSM) of design for cold-formed sections was recently extended in the North American Specification for Cold-Formed Steel Structural Members (NAS S100:2012) to include members in shear. The method has largely been developed on the basis of work done on lipped channel sections. To utilise the method requires the critical shear buckling load of the section, which may be determined from a minimum point on the signature curve for the section in pure shear. However when longitudinal web stiffeners are added to the channel a minimum may not exist, or may occur at half-wavelengths where the critical buckling mode is localised in the individual vertical portions of the web rather than involving the full web as an essentially continuous element, as occurs for a plain lipped channel in local shear buckling.

This paper explores the application of the recently-developed generalised constrained finite strip method (*c*FSM) to determine critical shear buckling loads for lipped channels with rectangular web stiffeners, from which shear buckling coefficients may be back-calculated. The addition of the stiffener leads to new distortional modes, deemed web-distortional modes, that play an important role in the buckling behaviour of web-stiffened channels at half-wavelengths where buckling involves deformations of the web as a continuous element. Using the *c*FSM, combinations of pure local modes and the web-distortional modes are considered to produce modal solutions. These modal solutions always give a minimum regardless of section and these minima are used to identify critical buckling half-wavelengths. The critical shear buckling loads are then taken as those at the same half-wavelengths on the corresponding traditional FSM signature curves for the sections. The proposed method is appropriate for sections with small stiffeners, as are used in practice.

[1] Ph.D. Candidate, [2] Emeritus Professor and [3] Associate Dean (Research and Research Training), School of Civil Engineering, The University of Sydney, Sydney NSW 2006, Australia.

Introduction

The Direct Strength Method (DSM) (Schafer and Peköz, 1998), incorporated in the North American Design Specification (NAS S100-2012; AISI 2012) and the Australian/New Zealand Standard for Cold-Formed Steel Structures (AS/NZS 4600:2005; Standards Australia 2005), is a method of design for cold-formed steel members that predicts the member capacity from the critical elastic buckling load and the material and geometric properties of the member. The critical elastic buckling load is determined from minima of the section's signature curve, generated by the finite strip method (FSM). The FSM was developed by Cheung (1968) and is a specialisation of the finite element method that utilises longitudinal regularity of the analysed member to reduce the dimension of the problem being analysed. It was first utilised for local buckling analysis of thin-walled members by Przemienicki (1973) and was extended to other forms of buckling by Plank and Wittrick (1974), in which form it was utilised by Hancock (1978) to develop curves of the critical elastic buckling load as a function of the buckling half-wavelength; i.e. the signature curve.

Recently, the DSM was extended in the North American Specification to include local buckling of members in shear (Pham and Hancock 2012a). For members where tension field action (TFA) is considered, the critical elastic shear buckling load may be determined by a spline FSM (SFSM) analysis (Pham and Hancock 2009, 2012b) or an FSM analysis with multiple series terms (Hancock and Pham 2013). Where TFA is not considered, the critical elastic shear buckling load may be determined from the minimum of the signature curve (Hancock and Pham 2012, Pham, Pham and Hancock 2014). A detailed study of web-stiffened channels in shear by Pham, Pham and Hancock (2012) revealed that the presence of the stiffeners often lead to signature curves that lack any minimum, hence complicating the selection of a critical buckling load for use in the DSM.

This problem of signature curves lacking minima is not unique to members under shear. In the DSM for members under compression and/or bending, two minima are usually expected, with that at smaller half-wavelengths corresponding to local buckling and the other to distortional buckling. However, there are many sections for which the signature curve may not have two minima, or may have more than one minimum for local or distortional buckling (Ádány 2004). Further, the buckling modes at such minima are not necessarily 'pure' local or distortional buckling. This prompted the development of the constrained finite strip method (*c*FSM) (Ádány and Schafer 2006a, b, 2008), which allows the buckling analysis to be restricted to consideration of certain 'pure' modes. By restricting analyses to consider only a combination of pure local and/or distortional modes, minima are regained on the modal solutions produced.

This paper applies the recently-developed generalised *c*FSM (Ádány and Schafer 2014a, b), extended to members in shear by Rendall, Hancock and Rasmussen (2016), to the analysis of lipped channels with rectangular web stiffeners in shear with the aim of determining critical elastic shear buckling loads. It briefly covers the current DSM design provisions for shear before providing an overview of the workings of the *c*FSM. The addition of the stiffener to the lipped channel gives rise to new distortional modes in the framework of the *c*FSM. The characteristics of these new modes, deemed web-distortional modes, are briefly elucidated. Modal solutions are produced using various combinations of pure local and/or web-distortional modes for a wide range of stiffener sizes. From these solutions critical half-wavelengths are selected and corresponding critical elastic shear buckling loads are determined. By studying the results of the various modal solutions, a coherent model is constructed for determination of the critical elastic shear buckling load for lipped channels with rectangular web stiffeners. The results of this model and the modal solutions are presented in the form of shear buckling coefficients.

Cross-section geometry and shear flow distribution

The geometry of the lipped channel section with a rectangular stiffener that will be analysed herein is shown in Fig. 1a. The section has a web depth of 200 mm (7.87”), a flange width of 80 mm (3.15”), a lip size of 20 mm (0.79”) and uniform thickness of 2 mm (0.08”). The section will be analysed for rectangular stiffeners with depths (b_{s1}) up to 190 mm (7.48”) and indents (b_{s2}) up to 50 mm (1.97”) all positioned symmetrically about the centre of the web. These dimensions are the same as those analysed by Pham, Pham and Hancock (2012).

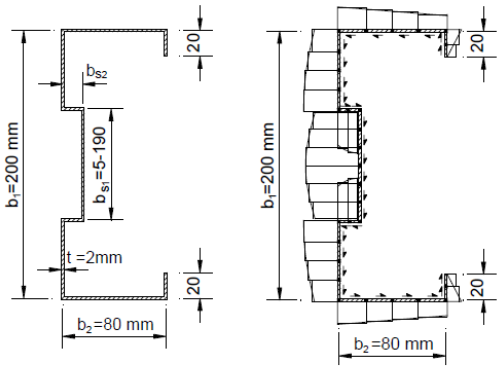

Figure 1: a) Geometry of web-stiffened channels and b) shear flow distribution (Pham, Pham and Hancock 2012)

For analysis in the FSM, the sections are divided into longitudinal strips. Regardless of stiffener size, the lips are split into 2 equal strips each and the flanges into 10 equal strips each. The vertical portions of the web that sit flush with the ends of the flanges are split into strips of 10 mm (0.39") width, with strips of 5 mm (0.20") width added just before the stiffener if necessary. Each of the three elements of the stiffener are split into either 4 equal strips or strips of 10 mm (0.39") width, whichever produces a finer division. The material properties are assumed to be isotropic with a Young's modulus of 200000 MPa (29008 kpsi) and a Poisson's ratio of 0.3.

Each section is subject to a shear flow distribution corresponding to that arising from a vertical shear load applied through the shear centre of the section; an example is shown in Fig. 1b. Note that such loading cannot exist without a moment gradient, which the FSM cannot capture, and so the analysed members may be said to be in a state of 'pure' shear. The FSM analysis utilised herein (for details, see Rendall, Hancock and Rasmussen 2016) is restricted to uniform shear stress in each strip, taken as the average of the true shear flow distribution over that strip. Hence a refined division of the section into strips, such as that utilised herein, provides a sufficient approximation to the true shear flow.

DSM design rules for pure shear

When tension field action is not considered, the nominal shear strength (V_n) of beams without holes in the web and without web stiffeners is determined from Appendix 1, Section 1.2.2.2.1 of NAS-2012 (AISI 2012) as follows:

$$\text{For } \lambda_v \leq 0.815: \; V_n = V_y \tag{1}$$

$$\text{For } 0.815 < \lambda_v \leq 1.227: \; V_n = 0.815\sqrt{V_{cr}V_y} \tag{2}$$

$$\text{For } \lambda_v > 1.227: \; V_n = V_{cr} \tag{3}$$

$$V_y = 0.6A_wF_y \tag{4}$$

where V_y is the yield load of the web (A_w is the area of the web) based on an average shear yield stress of $0.6F_y$ and V_{cr} is the elastic shear buckling force of the whole section, derived by integration of the shear stress distribution at buckling over the whole section; $\lambda_v = \sqrt{V_y/V_{cr}}$. Alternatively, V_{cr} may be determined from Eq. (5) if the appropriate shear buckling coefficient (k_v) of the whole section is known. In Eq. (5), E is Young's modulus, v is Poisson's ratio, d_1 is the depth of the flat portion of the web and t_w is the thickness of the web.

$$V_{cr} = \frac{k_v \pi^2 E A_w}{12\left(1-\nu^2\right)\left(d_1 / t_w\right)^2} \tag{5}$$

When tension field action is included, the nominal shear strength (V_n) of beams without holes is given by,

$$V_n = \left[1 - 0.15\left(\frac{V_{cr}}{V_y}\right)^{0.4}\right]\left(\frac{V_{cr}}{V_y}\right)^{0.4} V_y \tag{6}$$

It is desired to determine critical elastic shear buckling loads from which shear buckling coefficients may be back-calculated. For web-stiffened channels, the exact definitions of the web area and the depth of the flat portion of the web become unclear. Herein, the depth of the flat portion of the web will be taken as the sum of the vertical flats in the web and stiffener, resulting in $d_1 = b_1$, while the web area will simply be taken as this depth multiplied by the web thickness; i.e. $A_w = b_1 t_w$. Putting both of these definitions into Eq. (5) and rearranging then defines the shear buckling coefficient to be,

$$k_v = \frac{\left(V_{cr,FSM}\right)\cdot 12\left(1-\nu^2\right) b_1}{\pi^2 E t_w^3} \tag{7}$$

where $V_{cr,FSM}$ is the critical elastic shear buckling load, determined from the FSM at a half-wavelength determined by application of the *c*FSM.

Overview of the *c*FSM

The basic concept of the constrained finite strip method is that any general FSM displacement field **d** may be transformed to a constrained deformation space **M** by use of a constraint matrix $\mathbf{R_M}$, whose columns are base vectors of the constrained space. The original vector and that of the constrained deformation space ($\mathbf{d_M}$) are related by,

$$\mathbf{d} = \mathbf{R_M} \mathbf{d_M} . \tag{8}$$

By applying this transformation to the eigenvalue problem of the FSM, modal decomposition is achieved in that the resulting eigenmodes are constrained to the desired deformation space. The resulting eigenvalue problem is as given in Eq. (9). The constraint matrices act to reduce the size of the problem and so their

application to the global stiffness matrix ($\mathbf{K_E}$) and global stability matrix ($\mathbf{K_G}$) result in reduced-size matrices, particular to the current modal space. The matrices $\mathbf{\Lambda_M}$ and $\mathbf{\Theta_M}$ are, respectively, a diagonal matrix of load factors and a square matrix whose columns are the corresponding buckling modes in the reduced deformation space.

$$\left(\mathbf{R}_\mathbf{M}^\mathrm{T}\mathbf{K_E}\mathbf{R_M} - \mathbf{\Lambda_M}\mathbf{R}_\mathbf{M}^\mathrm{T}\mathbf{K_G}\mathbf{R_M}\right)\mathbf{\Theta_M} = \mathbf{0} \rightarrow \left(\mathbf{K_{E,M}} - \mathbf{\Lambda_M}\mathbf{K_{G,M}}\right)\mathbf{\Theta_M} = \mathbf{0} \tag{9}$$

Formulation of the constraint matrices is not covered here (see Ádány and Schafer 2014a, b) however, as the pure local and distortional modes are of interest in the current work, a brief description of their defining characteristics in the *c*FSM is now given. The pure local modes are defined by having null transverse extension, in-plane shear strain and longitudinal normal strain, which results in modes that allow only rotations at plate junctions and allow rotations and local out-of-plane deflection elsewhere. This definition of the local modes does not allow movement of the stiffener as a continuation of the web, as occurs in local buckling for sections with small stiffeners (Pham, Pham and Hancock 2012) hence the distortional modes, which do allow such movement of the stiffener, become of interest. The pure distortional modes are defined by null transverse extension and in-plane shear strain and by transverse displacements such that the cross-section satisfies transverse equilibrium as a frame.

The theoretical formulation of the stiffness and stability matrices is given in Rendall, Hancock and Rasmussen (2016). The utilised formulation assumes that the ends of the buckling half-wavelength are free to distort, hence the buckle is part of a very long length without restraint from end conditions.

Distortional modes of a lipped channel with a rectangular web stiffener

The transverse displacements of the distortional modes of a lipped channel with a rectangular stiffener, as determined by the *c*FSM, are shown in Fig. 2.

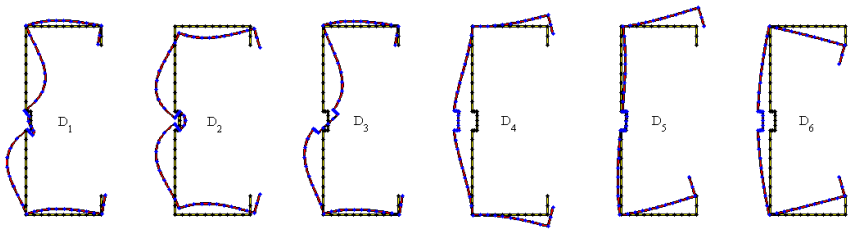

Figure 2: *c*FSM distortional modes of a lipped channel with a rectangular web

The last two of the modes, i.e. D_5 and D_6, shown in Fig. 2 respectively correspond to the usual anti-symmetric and symmetric distortional modes of a plain lipped channel. Since these two modes exist due to the presence of the lips as stiffeners on the flanges, they may be deemed flange-distortional modes. The addition of the rectangular stiffener in the web of the lipped channel gives rise to four additional distortional modes (D_1 to D_4 in Fig. 2), which may be deemed web-distortional modes. These four modes may be further split into two pairs, each consisting of one symmetric and one anti-symmetric mode. The first pair (D_1 and D_2) involve notable distortion of the stiffener, while the second pair (D_3 and D_4) involve a lesser degree of distortion in the stiffener. The distortion of the stiffener in the modes D_3 and D_4 is not noticeable in Fig. 2, which was produced for a stiffener with a depth of 20 mm (0.79") and indent of 5mm (0.20"), but is more prevalent for larger stiffener sizes, although the degree of distortion of the stiffener is greater in the modes D_1 and D_2 regardless of the stiffener size.

Shear buckling coefficients from individual modal solutions

In light of the pairs of new web-distortional modes, a total of three modal analyses shall be performed; one considering only the pure local (L) modes as defined by the *c*FSM, one considering the mode pair D_1 and D_2 and one considering the mode pair D_3 and D_4. As such, three modal solutions shall be produced for each section, each with its own distinct minimum. For the minimum of each modal solution, the half-wavelength at which it occurs shall be taken as a critical half-wavelength. The critical elastic shear buckling load is then taken as the result from the FSM signature curve at the same half-wavelength, from which a shear buckling coefficient is back-calculated using Eq. (7). An example of this process, up to determining the critical elastic shear buckling loads, is shown in Fig. 3 for a stiffener depth of 70 mm (2.76") and a stiffener indent of 15 mm (0.59"). Note that although the minimum critical loads of the distortional modal solutions lie significantly above the FSM solution (especially in the case of the mode pair D_1 and D_2), the minimum may still be used an as indicator of the half-wavelength at which the analysed modes may play their greatest role in the overall buckling mode.

Following this process, the shear buckling coefficients obtained for each section from modal solutions considering only the pure local modes are shown in Fig. 4. The coefficient at a stiffener depth of 0 mm (i.e. no stiffener) is 6.478, which is slightly lower than the 6.583 given by Pham, Pham and Hancock (2014), due to the more refined division of the cross-section; this minimum occurs at a half-wavelength of 196 mm.

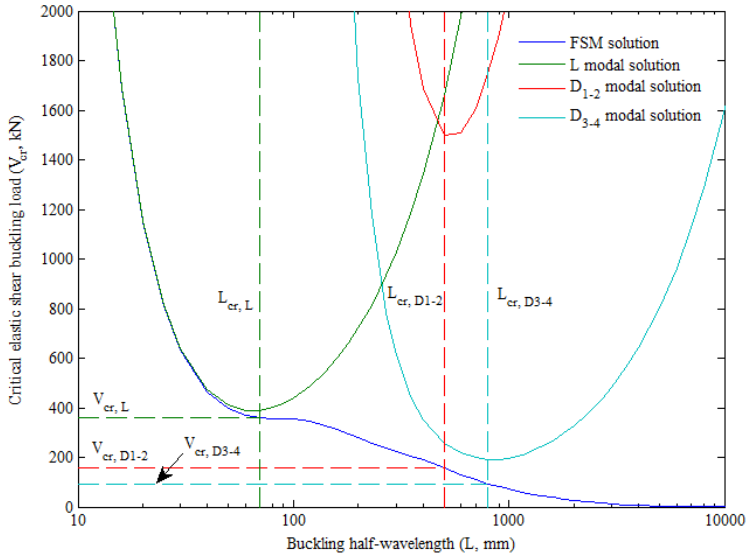

Figure 3: Identifying critical elastic shear buckling loads using critical half-wavelengths from modal *c*FSM solutions (b_{s1} = 70 mm, b_{s2} = 15 mm)

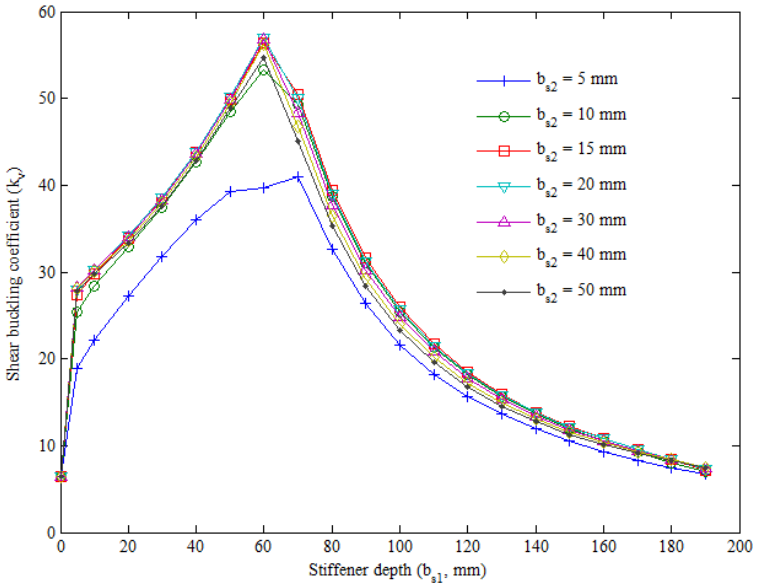

Figure 4: Shear buckling coefficients from considering local modes

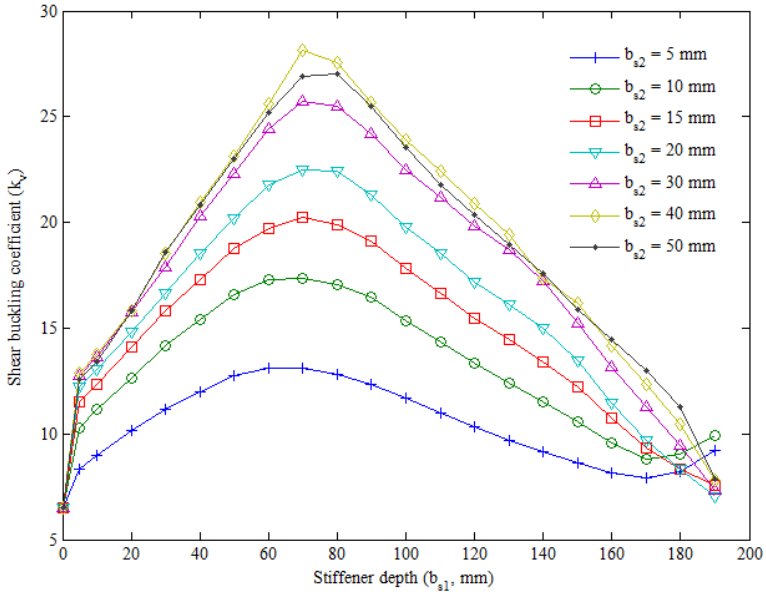

Figure 5: Shear buckling coefficients from considering modes D_1 and D_2

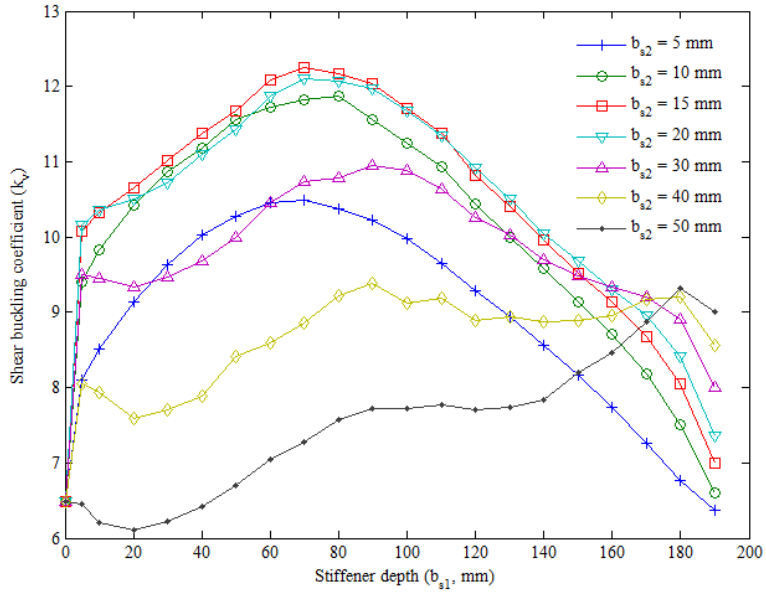

Figure 6: Shear buckling coefficients from considering modes D_3 and D_4

The shear buckling coefficients obtained from the local modal solutions display very similar behaviour regardless of the size of the stiffener indent, with the exception of the smallest indent, which has a significantly smaller shear buckling coefficient as the stiffener depth increases to 80 mm (3.15”). This discrepancy is due to stiffeners with such a small indent contributing little to the out-of-plane stiffness of the web and so leading to FSM solutions whose critical loads are smaller, at the half-wavelengths determined from the modal solutions, than those determined for stiffeners with larger indents. The initial drastic increase in the shear buckling coefficient as the stiffener depth becomes non-zero (i.e. as the section gains the stiffener) is due to the definition of the pure local modes in that the plate junctions may rotate but not deflect. Hence, in the limit as the stiffener depth approaches zero (for a sufficiently large stiffener indent), the section may be treated as equivalent to a plain lipped channel with the centre of the web simply-supported longitudinally, for which the shear buckling coefficient from the FSM solution is 23.304. For the stiffeners with indents of 10 mm (0.39”) or greater, the shear buckling coefficients increases in a quadratic fashion up to a maximum at a stiffener depth of 60 mm (2.36”), before decreasing in a similar manner as the stiffener depth is further increased. This behaviour is due to the local modal solution constraining the buckling to within individual elements of the web, hence the maximum shear buckling coefficient occurs where the maximum size of the individual elements is at their smallest; this occurs at a stiffener depth of between 60 and 70 mm (2.36 and 2.76”). Naturally then, the shear buckling coefficients become quite large, with the maximum of 56.923 being achieved for a stiffener of depth 60 mm (2.36”) and indent of 20 mm (0.79”), and the corresponding critical half-wavelengths from which the coefficients are determined are similar to the maximum depth of any of the vertical elements in the web.

The shear buckling coefficients obtained by considering the distortional mode pair D_1 and D_2 are shown in Fig. 5. As with the shear buckling coefficients in Fig. 4, those in Fig. 5 display a sudden increase as the stiffener is introduced, a general increase as the stiffener depth increases to 60-70 mm (2.36-2.76”) and then a general decrease as the stiffener depth is further increased. The trends of the increase and decrease are more linear in nature, except for a region near the maximum shear buckling coefficient for a given stiffener indent size, which becomes more localised around the maximum as the stiffener indent size increases. As noted in Pham, Pham and Hancock (2012), the addition of stiffeners of any size has a significantly smaller effect on increasing the distortional buckling load of the section than it does on increasing the local buckling load, hence leading to the shear buckling coefficients in Fig. 5 being generally significantly less than those in Fig. 4. The exceptions to this are those sections with large stiffener depths and indents, due to an increase in the critical

half-wavelength identified using this distortional mode pair. The maximum critical half-wavelength identified for a given stiffener indent varies from 320 mm (12.60") for the smallest indent to 950 mm (37.40") for the largest indent. For stiffener indents of, say, 15 mm (0.59") or greater, for which the identified half-wavelength is significantly larger than the web depth, the local shear buckling behaviour in the web is different than for a plain lipped channel and so assessing such sections using these modes may not be entirely appropriate.

The shear buckling coefficients obtained by considering the distortional mode pair D_3 and D_4 are shown in Fig. 6. The shear buckling coefficients obtained are significantly lower than those obtained from the two previous models, as the minima of the modal solutions considering this distortional mode pair occur at greater half-wavelengths. The maximum critical half-wavelength identified for a given stiffener indent varies from 490 mm (19.29") for the smallest indent to 1880 mm (74.02") for the largest indent. At such large half-wavelengths, any strength due to the stiffener is clearly lost, as evidenced by the coefficients for the sections with an indent of 50 mm (1.97") initially dropping with the introduction of the stiffener. Given the erratic variation of the shear buckling coefficients in this model, as well as the very large half-wavelengths at which minima may be identified, the model based on this distortional mode pair does not seem appropriate for identifying shear buckling coefficients.

A model for shear buckling coefficients

From the results presented, a model for determining shear buckling coefficients is developed as follows. As the pure local modes clearly characterise the buckling within each plate element, they must be included in such a model. The distortional mode pair D_1 and D_2 presents coherent and sensible results for shear buckling coefficients, while also occurring at the shortest half-wavelengths of the three distortional mode pairs, and so this mode pair will be included. This suggests a model based on considering the local modes and the distortional mode pair D_1 and D_2 simultaneously. However, in some instances, considering these modes together can lead to the loss of one of the two minima or to a minimum whose corresponding critical elastic shear buckling load is greater than that obtained by considering either the local modes or the distortional mode pair in isolation from the other. As such, the proposed model for determining shear buckling coefficients will determine three critical elastic shear buckling loads by considering i) the pure local modes only, ii) the distortional mode pair D_1 and D_2 and iii) the pure local modes and the distortional mode pair D_1 and D_2 simultaneously. The minimum load obtained will then be taken as the critical elastic shear buckling load for the section. The shear buckling coefficients obtained by this '$L - D_1 - D_2$' model are presented in Table 1.

Table 1: Shear buckling coefficients obtained by L – D_1 – D_2 model

Depth (mm)	Indent (mm)						
	5	10	15	20	30	40	50
5	8.313	10.260	11.500	12.246	12.740	12.887	12.567
10	8.987	11.155	12.354	13.052	13.620	13.734	13.416
20	10.152	12.661	14.110	14.823	15.756	15.827	15.796
30	11.184	14.178	15.827	16.620	17.901	18.559	18.594
40	12.008	15.418	17.294	18.513	20.275	20.955	20.829
50	12.744	16.587	18.738	20.177	22.323	23.147	23.029
60	13.135	17.285	19.688	21.749	24.429	25.617	25.170
70	13.118	17.348	20.255	22.500	25.702	28.155	26.922
80	12.827	17.067	19.907	22.425	25.505	27.548	26.994
90	12.333	16.478	19.097	21.319	24.192	25.689	25.504
100	11.675	15.337	17.850	19.772	22.472	23.907	23.346
110	10.969	14.363	16.666	18.532	20.811	20.152	19.596
120	10.311	13.317	15.492	17.177	17.729	17.197	16.739
130	9.716	12.412	14.473	15.797	15.335	14.893	14.509
140	9.141	11.495	13.389	13.804	13.428	13.057	12.741
150	8.612	10.588	12.209	12.160	11.879	11.575	11.313
160	8.175	9.597	10.737	10.791	10.592	10.351	10.140
170	7.936	8.788	9.318	9.583	9.479	9.309	9.150
180	7.372	8.064	8.342	8.302	8.446	8.369	8.274
190	6.732	6.949	7.173	7.062	7.348	7.444	7.413

In Table 1, the colour of each cell indicates which set of *c*FSM modes produces the critical elastic shear buckling load. Red indicates that considering the local modes only is critical, yellow indicates that considering the distortional mode pair D_1 and D_2 only is critical and orange indicates that considering both the local modes and the distortional modes pair D_1 and D_2 is critical. For most of the stiffeners analysed, the critical elastic shear buckling load comes from considering the distortional mode pair D_1 and D_2 only. However, as the stiffener depth and indent both become large, this usually changes to either of the other two obtained loads being critical.

There is a further consideration to be made for this model; namely, for sections where the FSM solution provides a minimum at short half-wavelengths for local buckling, such a minimum will obviously provide the smallest possible shear buckling coefficient at such half-wavelengths. If this buckling coefficient is considered in addition to the three determined previously, the results of such a 'L – D_1 – D_2 – FSM' model are given in Table 2.

Table 2: Shear buckling coefficients obtained by L – D_1 – D_2 – FSM model*

Depth	Indent (mm)						
(mm)	5	10	15	20	30	40	50
5	8.006	10.260	11.500	12.246	12.740	12.887	12.567
10	8.987	11.155	12.354	13.052	13.620	13.734	13.416
20	10.152	12.661	14.110	14.823	15.756	15.827	15.796
30	11.184	14.178	15.827	16.620	17.901	18.559	18.594
40	12.008	15.418	17.294	18.513	20.275	20.955	20.829
50	12.744	16.587	18.738	20.177	22.323	23.147	23.029
60	13.135	17.285	19.688	21.749	24.429	25.617	25.170
70	13.118	17.348	20.255	22.500	25.702	28.155	26.922
80	12.827	17.067	19.907	22.425	25.505	27.548	26.994
90	12.333	16.478	19.097	21.319	24.192	25.689	25.504
100	11.675	15.337	17.850	19.772	22.472	23.907	23.343
110	10.969	14.363	16.666	18.532	20.788	20.150	19.595
120	10.311	13.317	15.492	17.177	17.723	17.193	16.736
130	9.716	12.412	14.473	15.743	15.327	14.889	14.509
140	9.141	11.495	13.389	13.754	13.419	13.057	12.741
150	8.111	10.588	12.087	12.126	11.869	11.574	11.312
160	7.601	9.597	10.638	10.740	10.577	10.348	10.138
170	7.100	8.142	9.318	9.492	9.448	9.300	9.145
180	6.664	7.250	7.867	8.281	8.392	8.340	8.256
190	6.366	6.463	6.667	6.907	7.262	7.360	7.370

* Shaded cells are those for which the FSM solution is critical and hence the coefficient differs from that in the corresponding cell in Table 1.

The shaded cells in Table 2 indicate the sections for which the minimum from the FSM solution is critical; for these particular sections with stiffener indents of 20 mm (0.79") or more, the difference is less than 1% between Tables 1 and 2. For smaller stiffeners, the difference may be up to 10%. Of the remaining sections, the distortional mode pair D_1 and D_2 gives the critical solution in all but two cases; those with an indent of 50 mm (1.97") and depths of 130 and 140 mm (5.12 and 5.51").

Conclusions

This paper has explored application of the *c*FSM to the identification of shear buckling coefficients of lipped channels with rectangular web stiffeners experiencing local buckling. The pure local modes as determined by the *c*FSM were elucidated as being insufficient for identifying this mode for sections with stiffeners and so lead to a brief exploration of the pure distortional modes of

such a section. New web-distortional modes were identified and briefly analysed, leading to three separate models for identifying shear buckling coefficients. Two of the models presented coherent results and so these were merged to produce a combined model for determining shear buckling coefficients. This model was then updated to include shear buckling coefficients obtained from the minimum of the FSM signature curve, which gives the smallest possible shear buckling coefficient when examining short half-wavelengths. While this shear buckling coefficient was critical for a number of the sections, in many cases the difference was on the order of 1%. The developed model is appropriate for sections with small stiffener indents.

Appendix – References

Ádány, S. (2004). "Buckling mode classification of members with open thin-walled cross-sections by using the finite strip method." Research Report, Johns Hopkins University.

Ádány, S., Schafer, B.W. (2006a). "Buckling mode decomposition of single-branched open cross-section members via finite strip method: Derivation." *Thin-Walled Struct*. 44 (5) 563-584.

Ádány, S., Schafer, B.W. (2006b). "Buckling mode decomposition of single-branched open cross-section members via finite strip method: Applications and examples." *Thin-Walled Struct.* 44 (5) 585-600.

Ádány, S., Schafer, B.W. (2008). "A full modal decomposition of thin-walled, single-branched open cross-section members via the constrained finite strip method." *J. Constr. Steel Res.*, 64 (1) 12-29.

Ádány, S., Schafer, B.W. (2014a). "Generalized constrained finite strip method for thin-walled members with arbitrary cross-section: Primary modes." *Thin-Walled Struct.*, 84 150-169.

Ádány, S., Schafer, B.W. (2014b). "Generalized constrained finite strip method for thin-walled members with arbitrary cross-section: Secondary modes, orthogonality, examples." *Thin-Walled Struct.,* 84 123-133.

American Iron and Steel Institute (AISI) (2012). North American specification for the design of cold-formed steel structural members [2012 Ed.]. AISI S100-2012.

Cheung, Y.K. (1968). “Finite strip method in the analysis of elastic plates with two opposite ends.” *ICE Proc.*, 40 (1) 1–7.

Hancock, G.J. (1978). “Local, distortional, and lateral buckling of I-beams.” *ASCE J. Struct. Div.*, 104 (11) 1787-1798.

Hancock, G.J., Pham, C.H. (2012). “Direct Strength Method of design for shear of cold-formed channels based on a shear signature curve.” *Proc. 21st Int. Spec. Conf. on Cold-Formed Steel Struct.*.

Hancock, G.J., Pham, C.H. (2013). “Shear buckling of channel sections with simply supported ends using the Semi-Analytical Finite Strip Method.” *Thin-Walled Struct.*, 71 72-80.

Pham, C.H., Hancock, G.J. (2009). “Shear buckling of thin-walled channel sections.” *J. Constr. Steel Res.* 65 (3) 578-585.

Pham, C.H., Hancock, G.J. (2012a). “Direct strength design of cold-formed C-sections for shear and combined actions.” *ASCE J. Struct. Eng.*, 138 (6) 759-768.

Pham, C.H., Hancock, G.J. (2012b). “Elastic buckling of cold-formed channel sections in shear.” *Thin-Walled Struct.* 61 22-26.

Pham, S.H., Pham, C.H., Hancock, G.J. (2012). “Shear buckling of thin-walled channels sections with complex stiffened webs.” *Proc. 21st Int. Spec. Conf. on Cold-Formed Steel Struct.*.

Pham, S.H., Pham, C.H., Hancock, G.J. (2014). “Direct strength method of design for shear including sections with longitudinal web stiffeners.” *Thin-Walled Struct.*, 81 19-28.

Plank, R.J., Wittrick, W.H. (1974). “Buckling under combined loading of thin, flat-walled structures by a complex finite strip method.” *Int. J. Numer. Meth. Eng.*, 8 (2) 323-339.

Przemieniecki, J.S. (1973). “Finite element structural analysis of local instability.” *AIAA J.*, 11 (1) 33-39.

Rendall, M.A., Hancock, G.J., Rasmussen, K.J.R. (2016). “The generalised constrained finite strip method for thin-walled, prismatic members under applied shear.” Research Report R963, The University of Sydney.

Schafer, B.W., Peköz, T. (1998). "Direct strength prediction of cold-formed steel members using numerical elastic buckling solutions." *Proc. 14th Int. Spec. Conf. on Cold-Formed Steel Struct. St. Louis, Missouri*, 69-76.

Standards Australia (2005). AS/NZS 4600, Cold-Formed Steel Structures. Standards Australia/Standards New Zealand.